FERMILAB-PUB-16-234-ND

# Limits on Active to Sterile Neutrino Oscillations from Disappearance Searches in the MINOS, Daya Bay, and Bugey-3 Experiments

P. Adamson[μ,1] F. P. An[δ,2] I. Anghel[μ,3,4] A. Aurisano[μ,5] A. B. Balantekin[δ,6] H. R. Band[δ,7] G. Barr[μ,8] M. Bishai[δμ,9] A. Blake[μ,10,11] S. Blyth[δ,12,13] G. J. Bock[μ,1] D. Bogert[μ,1] D. Cao[δ,14] G. F. Cao[δ,15] J. Cao[δ,15] S. V. Cao[μ,16] T. J. Carroll[μ,16] C. M. Castromonte[μ,17] W. R. Cen[δ,15] Y. L. Chan[δ,18] J. F. Chang[δ,15] L. C. Chang[δ,19] Y. Chang[δ,13] H. S. Chen[δ,15] Q. Y. Chen[δ,20] R. Chen[μ,21] S. M. Chen[δ,22] Y. Chen[δ,23] Y. X. Chen[δ,24] J. Cheng[δ,20] J.-H. Cheng[δ,19] Y. P. Cheng[δ,15] Z. K. Cheng[δ,25] J. J. Cherwinka[δ,6] S. Childress[μ,1] M. C. Chu[δ,18] A. Chukanov[δ,26] J. A. B. Coelho[μ,27] L. Corwin[μ,28] D. Cronin-Hennessy[μ,29] J. P. Cummings[δ,30] J. de Arcos[δ,31] S. De Rijck[μ,16] Z. Y. Deng[δ,15] A. V. Devan[μ,32] N. E. Devenish[μ,33] X. F. Ding[δ,15] Y. Y. Ding[δ,15] M. V. Diwan[δμ,9] M. Dolgareva[δ,26] J. Dove[δ,34] D. A. Dwyer[δ,35] W. R. Edwards[δ,35] C. O. Escobar[μ,36] J. J. Evans[μ,21] E. Falk[μ,33] G. J. Feldman[μ,37] W. Flanagan[μ,16] M. V. Frohne[μ,38,*] M. Gabrielyan[μ,29] H. R. Gallagher[μ,27] S. Germani[μ,39] R. Gill[δ,9] R. A. Gomes[μ,17] M. Gonchar[δ,26] G. H. Gong[δ,22] H. Gong[δ,22] M. C. Goodman[μ,4] P. Gouffon[μ,40] N. Graf[μ,41] R. Gran[μ,42] M. Grassi[δ,15] K. Grzelak[μ,43] W. Q. Gu[δ,44] M. Y. Guan[δ,15] L. Guo[δ,22] R. P. Guo[δ,15] X. H. Guo[δ,45] Z. Guo[δ,22] A. Habig[μ,42] R. W. Hackenburg[δ,9] S. R. Hahn[μ,1] R. Han[δ,24] S. Hans[δ,9,†] J. Hartnell[μ,33] R. Hatcher[μ,1] M. He[δ,15] K. M. Heeger[δ,7] Y. K. Heng[δ,15] A. Higuera[δ,46] A. Holin[μ,39] Y. K. Hor[δ,47] Y. B. Hsiung[δ,12] B. Z. Hu[δ,12] T. Hu[δ,15] W. Hu[δ,15] E. C. Huang[δ,34] H. X. Huang[δ,48] J. Huang[μ,16] X. T. Huang[δ,20] P. Huber[δ,47] W. Huo[δ,49] G. Hussain[δ,22] J. Hylen[μ,1] G. M. Irwin[μ,50] Z. Isvan[μ,9] D. E. Jaffe[δ,9] P. Jaffke[δ,47] C. James[μ,1] K. L. Jen[δ,19] D. Jensen[μ,1] S. Jetter[δ,15] X. L. Ji[δ,15] X. P. Ji[δ,51,22] J. B. Jiao[δ,20] R. A. Johnson[δ,52] J. K. de Jong[μ,8] J. Joshi[δ,9] T. Kafka[μ,27] L. Kang[δ,53] S. M. S. Kasahara[μ,29] S. H. Kettell[δ,9] S. Kohn[δ,54] G. Koizumi[μ,1] M. Kordosky[μ,32] M. Kramer[δ,35,54] A. Kreymer[μ,1] K. K. Kwan[δ,18] M. W. Kwok[δ,18] T. Kwok[δ,55] K. Lang[μ,16] T. J. Langford[δ,7] K. Lau[δ,46] L. Lebanowski[δ,22] J. Lee[δ,35] J. H. C. Lee[δ,55] R. T. Lei[δ,53] R. Leitner[δ,56] J. K. C. Leung[δ,55] C. Li[δ,20] D. J. Li[δ,49] F. Li[δ,15] G. S. Li[δ,44] Q. J. Li[δ,15] S. Li[δ,53] S. C. Li[δ,55,47] W. D. Li[δ,15] X. N. Li[δ,15] Y. F. Li[δ,15] Z. B. Li[δ,25] H. Liang[δ,49] C. J. Lin[δ,35] G. L. Lin[δ,19] S. Lin[δ,53] S. K. Lin[δ,46] Y.-C. Lin[δ,12] J. J. Ling[δμ,25,9] J. M. Link[δ,47] P. J. Litchfield[μ,29,57] L. Littenberg[δ,9] B. R. Littlejohn[δ,31] D. W. Liu[δ,46] J. C. Liu[δ,15] J. L. Liu[δ,44] C. W. Loh[δ,14] C. Lu[δ,58] H. Q. Lu[δ,15] J. S. Lu[δ,15] P. Lucas[μ,1] K. B. Luk[δ,54,35] Z. Lv[δ,59] Q. M. Ma[δ,15] X. B. Ma[δ,24] X. Y. Ma[δ,15] Y. Q. Ma[δ,15] Y. Malyshkin[δ,60] W. A. Mann[μ,27] M. L. Marshak[μ,29] D. A. Martinez Caicedo[δ,31] N. Mayer[μ,27] K. T. McDonald[δ,58] C. McGivern[μ,41] R. D. McKeown[δ,61,32] M. M. Medeiros[μ,17] R. Mehdiyev[μ,16] J. R. Meier[μ,29] M. D. Messier[μ,28] W. H. Miller[μ,29] S. R. Mishra[μ,62] I. Mitchell[δ,46] M. Mooney[δ,9] C. D. Moore[μ,1] L. Mualem[μ,61] J. Musser[μ,28] Y. Nakajima[δ,35] D. Naples[μ,41] J. Napolitano[δ,63] D. Naumov[δ,26] E. Naumova[δ,26] J. K. Nelson[μ,32] H. B. Newman[μ,61] H. Y. Ngai[δ,55] R. J. Nichol[μ,39] Z. Ning[δ,15] J. A. Nowak[μ,29] J. O'Connor[μ,39] J. P. Ochoa-Ricoux[δ,60] A. Olshevskiy[δ,26] M. Orchanian[μ,61] R. B. Pahlka[μ,1] J. Paley[μ,4] H.-R. Pan[δ,12] J. Park[δ,47] R. B. Patterson[μ,61] S. Patton[δ,35] G. Pawloski[μ,29] V. Pec[δ,56] J. C. Peng[δ,34] A. Perch[μ,39] M. M. Pfützner[μ,39] D. D. Phan[μ,16] S. Phan-Budd[μ,4] L. Pinsky[δ,46] R. K. Plunkett[μ,1] N. Poonthottathil[μ,1] C. S. J. Pun[δ,55] F. Z. Qi[δ,15] M. Qi[δ,14] X. Qian[δ,9] X. Qiu[μ,50] A. Radovic[μ,32] N. Raper[δ,64] B. Rebel[μ,1] J. Ren[δ,48] C. Rosenfeld[μ,62] R. Rosero[δ,9] B. Roskovec[δ,56] X. C. Ruan[δ,48] H. A. Rubin[μ,31] P. Sail[μ,16] M. C. Sanchez[μ,3,4] J. Schneps[μ,27] A. Schreckenberger[μ,16] P. Schreiner[μ,4] R. Sharma[μ,1] S. Moed Sher[μ,1] A. Sousa[μ,5] H. Steiner[δ,54,35] G. X. Sun[δ,15] J. L. Sun[δ,65] N. Tagg[μ,66] R. L. Talaga[μ,4] W. Tang[δ,9] D. Taychenachev[δ,26] J. Thomas[μ,39] M. A. Thomson[μ,10] X. Tian[μ,62] A. Timmons[μ,21] J. Todd[μ,5] S. C. Tognini[μ,17] R. Toner[μ,37] D. Torretta[μ,1] K. Treskov[δ,26] K. V. Tsang[δ,35] C. E. Tull[δ,35] G. Tzanakos[μ,67,*] J. Urheim[μ,28] P. Vahle[μ,32] N. Viaux[δ,60] B. Viren[δμ,9] V. Vorobel[δ,56] C. H. Wang[δ,13] M. Wang[δ,20] N. Y. Wang[δ,45] R. G. Wang[δ,15] W. Wang[δ,32,25] X. Wang[δ,68] Y. F. Wang[δ,15] Z. Wang[δ,15] Z. M. Wang[δ,15] R. C. Webb[μ,69] A. Weber[μ,8,57] H. Y. Wei[δ,22] L. J. Wen[δ,15] K. Whisnant[δ,3] C. White[δμ,31] L. Whitehead[δμ,46] L. H. Whitehead[μ,39] T. Wise[δ,6] S. G. Wojcicki[μ,50] H. L. H. Wong[δ,54,35] S. C. F. Wong[δ,25] E. Worcester[δ,9] C.-H. Wu[δ,19] Q. Wu[δ,20] W. J. Wu[δ,15] D. M. Xia[δ,70] J. K. Xia[δ,15] Z. Z. Xing[δ,15] J. L. Xu[δ,15] J. Y. Xu[δ,18] Y. Xu[δ,25] T. Xue[δ,22] C. G. Yang[δ,15] H. Yang[δ,14] L. Yang[δ,53] M. S. Yang[δ,15] M. T. Yang[δ,20] M. Ye[δ,15] Z. Ye[δ,46] M. Yeh[δ,9] B. L. Young[δ,3] Z. Y. Yu[δ,15] S. Zeng[δ,15] L. Zhan[δ,15] C. Zhang[δ,9] H. H. Zhang[δ,25] J. W. Zhang[δ,15] Q. M. Zhang[δ,59] X. T. Zhang[δ,15] Y. M. Zhang[δ,25] Y. X. Zhang[δ,65] Z. J. Zhang[δ,53] Z. P. Zhang[δ,49] Z. Y. Zhang[δ,15] J. Zhao[δ,15] Q. W. Zhao[δ,15] Y. B. Zhao[δ,15] W. L. Zhong[δ,15] L. Zhou[δ,15] N. Zhou[δ,49] H. L. Zhuang[δ,15] and J. H. Zou[δ15]

([δ]Daya Bay Collaboration)

([μ]MINOS Collaboration)

[1]*Fermi National Accelerator Laboratory, Batavia, Illinois 60510, USA*
[2]*Institute of Modern Physics, East China University of Science and Technology, Shanghai*
[3]*Department of Physics and Astronomy, Iowa State University, Ames, Iowa 50011 USA*
[4]*Argonne National Laboratory, Argonne, Illinois 60439, USA*
[5]*Department of Physics, University of Cincinnati, Cincinnati, Ohio 45221, USA*

arXiv:1607.01177v3 [hep-ex] 8 Jul 2016

[6]*Physics Department, University of Wisconsin, Madison, Wisconsin 53706, USA*
[7]*Department of Physics, Yale University, New Haven, Connecticut 06520, USA*
[8]*Subdepartment of Particle Physics, University of Oxford, Oxford OX1 3RH, United Kingdom*
[9]*Brookhaven National Laboratory, Upton, New York 11973, USA*
[10]*Cavendish Laboratory, University of Cambridge,Cambridge CB3 0HE, United Kingdom*
[11]*Lancaster University, Lancaster, LA1 4YB, UK*
[12]*Department of Physics, National Taiwan University, Taipei*
[13]*National United University, Miao-Li*
[14]*Nanjing University, Nanjing*
[15]*Institute for High Energy Physics, Protvino, Moscow Region RU-140284, Russia*
[16]*Department of Physics, University of Texas at Austin, Austin, Texas 78712, USA*
[17]*Instituto de Física, Universidade Federal de Goiás, 74690-900, Goiânia, GO, Brazil*
[18]*Chinese University of Hong Kong, Hong Kong*
[19]*Institute of Physics, National Chiao-Tung University, Hsinchu*
[20]*Shandong University, Jinan*
[21]*School of Physics and Astronomy, University of Manchester, Manchester M13 9PL, United Kingdom*
[22]*Department of Engineering Physics, Tsinghua University, Beijing*
[23]*Shenzhen University, Shenzhen*
[24]*North China Electric Power University, Beijing*
[25]*Sun Yat-Sen (Zhongshan) University, Guangzhou*
[26]*Joint Institute for Nuclear Research, Dubna, Moscow Region*
[27]*Physics Department, Tufts University, Medford, Massachusetts 02155, USA*
[28]*Indiana University, Bloomington, Indiana 47405, USA*
[29]*University of Minnesota, Minneapolis, Minnesota 55455, USA*
[30]*Siena College, Loudonville, New York 12211, USA*
[31]*Department of Physics, Illinois Institute of Technology, Chicago, Illinois 60616, USA*
[32]*Department of Physics, College of William & Mary, Williamsburg, Virginia 23187, USA*
[33]*Department of Physics and Astronomy, University of Sussex, Falmer, Brighton BN1 9QH, United Kingdom*
[34]*Department of Physics, University of Illinois at Urbana-Champaign, Urbana, Illinois 61801, USA*
[35]*Lawrence Berkeley National Laboratory, Berkeley, California, 94720 USA*
[36]*Universidade Estadual de Campinas, IFGW, CP 6165, 13083-970, Campinas, SP, Brazil*
[37]*Department of Physics, Harvard University, Cambridge, Massachusetts 02138, USA*
[38]*Holy Cross College, Notre Dame, Indiana 46556, USA*
[39]*Department of Physics and Astronomy, University College London, London WC1E 6BT, United Kingdom*
[40]*Instituto de Física, Universidade de São Paulo, CP 66318, 05315-970, São Paulo, SP, Brazil*
[41]*Department of Physics and Astronomy, University of Pittsburgh, Pittsburgh, Pennsylvania 15260, USA*
[42]*Department of Physics, University of Minnesota Duluth, Duluth, Minnesota 55812, USA*
[43]*Department of Physics, University of Warsaw,PL-02-093 Warsaw, Poland*
[44]*Department of Physics and Astronomy, Shanghai Jiao Tong University, Shanghai Laboratory for Particle Physics and Cosmology, Shanghai*
[45]*Beijing Normal University, Beijing*
[46]*Department of Physics, University of Houston, Houston, Texas 77204, USA*
[47]*Center for Neutrino Physics, Virginia Tech, Blacksburg, Virginia 24061, USA*
[48]*China Institute of Atomic Energy, Beijing*
[49]*University of Science and Technology of China, Hefei*
[50]*Department of Physics, Stanford University, Stanford, California 94305, USA*
[51]*School of Physics, Nankai University, Tianjin*
[52]*Department of Physics, University of Cincinnati, Cincinnati, Ohio 45221, USA*
[53]*Dongguan University of Technology, Dongguan*
[54]*Department of Physics, University of California, Berkeley, California 94720, USA*
[55]*Department of Physics, The University of Hong Kong, Pokfulam, Hong Kong*
[56]*Charles University, Faculty of Mathematics and Physics, Prague, Czech Republic*
[57]*Rutherford Appleton Laboratory, Science and Technology Facilities Council, Didcot, OX11 0QX, United Kingdom*
[58]*Joseph Henry Laboratories, Princeton University, Princeton, New Jersey 08544, USA*
[59]*Xi'an Jiaotong University, Xi'an*
[60]*Instituto de Física, Pontificia Universidad Católica de Chile, Santiago, Chile*
[61]*Lauritsen Laboratory, California Institute of Technology, Pasadena, California 91125, USA*
[62]*Department of Physics and Astronomy, University of South Carolina, Columbia, South Carolina 29208, USA*
[63]*Department of Physics, College of Science and Technology, Temple University, Philadelphia, Pennsylvania 19122, USA*
[64]*Department of Physics, Applied Physics, and Astronomy, Rensselaer Polytechnic Institute, Troy, New York 12180, USA*
[65]*China General Nuclear Power Group*
[66]*Otterbein University, Westerville, Ohio 43081, USA*
[67]*Department of Physics, University of Athens, GR-15771 Athens, Greece*
[68]*College of Electronic Science and Engineering, National University of Defense Technology, Changsha*
[69]*Physics Department, Texas A&M University, College Station, Texas 77843, USA*

[70]*Chongqing University, Chongqing*
(Dated: July 11, 2016)

Searches for a light sterile neutrino have been independently performed by the MINOS and the Daya Bay experiments using the muon (anti)neutrino and electron antineutrino disappearance channels, respectively. In this Letter, results from both experiments are combined with those from the Bugey-3 reactor neutrino experiment to constrain oscillations into light sterile neutrinos. The three experiments are sensitive to complementary regions of parameter space, enabling the combined analysis to probe regions allowed by the LSND and MiniBooNE experiments in a minimally extended four-neutrino flavor framework. Stringent limits on $\sin^2 2\theta_{\mu e}$ are set over six orders of magnitude in the sterile mass-squared splitting $\Delta m^2_{41}$. The sterile-neutrino mixing phase space allowed by the LSND and MiniBooNE experiments is excluded for $\Delta m^2_{41} < 0.8$ eV$^2$ at 95% C.L.

PACS numbers: 14.60.Pq, 29.40.Mc, 28.50.Hw, 13.15.+g
Keywords: light sterile neutrino, MINOS, Daya Bay

The discovery of neutrino flavor oscillations [1, 2] marked a crucial milestone in the history of particle physics. It indicates neutrinos undergo mixing between flavor and mass eigenstates and hence carry non-zero mass. It also represents the first evidence of physics beyond the Standard Model of particle physics. Since then, neutrino oscillations have been confirmed and precisely measured with data from natural (atmospheric and solar) and man-made (reactor and accelerator) neutrino sources.

The majority of neutrino oscillation data available can be well described by a three-flavor neutrino model [3–5] in agreement with precision electroweak measurements from collider experiments [6, 7]. A few experimental results, however, including those from LSND [8] and MiniBooNE [9], cannot be explained by three-neutrino mixing. Both experiments observed an electron antineutrino excess in a muon antineutrino beam over short baselines, suggesting mixing with a new neutrino state with mass-squared splitting $\Delta m^2_{41} \gg |\Delta m^2_{32}|$, where $\Delta m^2_{ji} \equiv m^2_j - m^2_i$, and $m_i$ is the mass of the $i^{\rm th}$ mass eigenstate. Precision electroweak measurements exclude standard couplings of this additional neutrino state for masses up to half the $Z$-boson mass, so that states beyond the known three active states are referred to as *sterile*. New light neutrino states would open a new sector in particle physics, thus confirming or refuting these results is at the forefront of neutrino physics research.

Mixing between one or more light sterile neutrinos and the active neutrino flavors would have discernible effects on neutrino oscillation measurements. Oscillations from muon to electron (anti)neutrinos driven by a sterile neutrino require electron and muon neutrino flavors to couple to the additional neutrino mass eigenstates. Consequently, oscillations between active and sterile states will also necessarily result in disappearance of muon (anti)neutrinos, as well as of electron (anti)neutrinos, independently of the sterile neutrino model considered [10, 11].

In this Letter, we report results from a joint analysis developed in parallel to the independent sterile neutrino searches from Daya Bay [12] and MINOS [13]. In this analysis, the measurement of muon (anti)neutrino disappearance by MINOS is combined with electron antineutrino disappearance measurements from Daya Bay and Bugey-3 [14] using the $\mathrm{CL_s}$ method [15, 16]. The combined results are analyzed in light of the muon (anti)neutrino to electron (anti)neutrino appearance indications from LSND [8] and MiniBooNE [9]. The independent MINOS, Daya Bay, and Bugey-3 results are all obtained from disappearance measurements and therefore are insensitive to CP-violating effects due to mixing between the three active flavors. Under the assumption of CPT invariance, the combined results shown constrain both neutrino and antineutrino appearance.

The results reported here required several novel improvements developed independently from the Daya Bay-only [12] and MINOS-only [13] analyses, specifically: a full re-analysis of the MINOS data to search for sterile neutrino mixing, based on the $\mathrm{CL_s}$ method; a $\mathrm{CL_s}$-based analysis of Bugey-3 results taking into account new reactor flux calculations and Daya Bay's reactor flux measurement; the combination of Daya Bay results with Bugey-3 results taking into account correlated systematics between the experiments; and, finally, the combination of the Daya Bay/Bugey-3 and MINOS results to place stringent constraints on electron neutrino and antineutrino appearance driven by sterile neutrino oscillations.

We adopt a minimal extension of the three-flavor neutrino model by including one sterile flavor and one additional mass eigenstate. This 3+1 sterile neutrino scenario is referred to as the *four-flavor model* in the text. In this model, the appearance probability of muon to electron neutrino, $P_{\nu_\mu\to\nu_e}(L/E)$ as a function of the propagation length, $L$, divided by the neutrino energy, $E$, can be expressed using a 4×4 unitary mixing matrix, $U$, by

$$P_{\nu_\mu\to\nu_e}(L/E) = \mathrm{Re}\left(\sum_j\sum_{j\neq k} U_{\mu j}U^*_{ej}U^*_{\mu k}U_{ek}e^{i\frac{\Delta m^2_{jk}L}{2E}}\right). \tag{1}$$

In the region where $\Delta m^2_{41} \gg |\Delta m^2_{32}|$, Eq. (1) can be simplified to

$$P_{\nu_\mu\to\nu_e}(L/E) \approx 4|U_{\mu 4}|^2|U_{e4}|^2\sin^2\left(\frac{\Delta m^2_{41}L}{4E}\right) \approx P_{\bar{\nu}_\mu\to\bar{\nu}_e}. \tag{2}$$

A non-zero amplitude, $4|U_{\mu 4}|^2|U_{e4}|^2$, of the appearance probability is a possible explanation for the MiniBooNE

and LSND results. The matrix element $|U_{e4}|^2$ can be constrained with measurements of electron antineutrino disappearance, as in the Daya Bay [12] and Bugey-3 [14] experiments. Likewise, $|U_{\mu 4}|^2$ can be constrained with measurements of muon neutrino and antineutrino disappearance, as in the MINOS [13] experiment. The survival probabilities $P_{\bar{\nu}_e \to \bar{\nu}_e}(L/E)$ and $P_{\overset{(-)}{\nu}_\mu \to \overset{(-)}{\nu}_\mu}(L/E)$ are

$$P_{\bar{\nu}_e \to \bar{\nu}_e}(L/E) = 1 - 4 \sum_{k>j} |U_{ek}|^2 |U_{ej}|^2 \sin^2 \left( \frac{\Delta m^2_{kj} L}{4E} \right), \tag{3}$$

$$P_{\overset{(-)}{\nu}_\mu \to \overset{(-)}{\nu}_\mu}(L/E) = 1 - 4 \sum_{k>j} |U_{\mu k}|^2 |U_{\mu j}|^2 \sin^2 \left( \frac{\Delta m^2_{kj} L}{4E} \right). \tag{4}$$

The mixing matrix augmented with one sterile state can be parameterized by

$U = R_{34} R_{24} R_{14} R_{23} R_{13} R_{12}$ [17], where $R_{ij}$ is the rotational matrix for the mixing angle $\theta_{ij}$, yielding

$$\begin{aligned} |U_{e4}|^2 &= \sin^2 \theta_{14}, \\ |U_{\mu 4}|^2 &= \sin^2 \theta_{24} \cos^2 \theta_{14}, \\ 4|U_{e4}|^2 |U_{\mu 4}|^2 &= \sin^2 2\theta_{14} \sin^2 \theta_{24} \equiv \sin^2 2\theta_{\mu e}. \end{aligned} \tag{5}$$

Searches for sterile neutrinos are carried out by using the reconstructed energy spectra to look for evidence of oscillations driven by the sterile mass-squared difference $\Delta m^2_{41}$. For small values of $\Delta m^2_{41}$, corresponding to slow oscillations, the energy-dependent shape of the oscillation probability could be measured in the reconstructed energy spectra. For large values corresponding to rapid oscillations, an overall reduction in neutrino flux would be seen.

The $\mathrm{CL_s}$ method [15, 16] is a two-hypothesis test that compares the three-flavor (null) hypothesis (labeled $3\nu$) to an alternate four-flavor hypothesis (labeled $4\nu$). To determine if the four-flavor hypothesis can be excluded, we construct the test statistic $\Delta\chi^2 = \chi^2_{4\nu} - \chi^2_{3\nu}$, where $\chi^2_{4\nu}$ is the $\chi^2$ value resulting from a fit to a four-flavor hypothesis, and $\chi^2_{3\nu}$ is the $\chi^2$ value from a fit to the three-flavor hypothesis. The $\Delta\chi^2$ observed with data, $\Delta\chi^2_{\mathrm{obs}}$, is compared to the $\Delta\chi^2$ distributions expected if the three-flavor hypothesis is true, or the four-flavor hypothesis is true. To quantify this, we construct

$$\begin{aligned} \mathrm{CL_b} &= P(\Delta\chi^2 \geq \Delta\chi^2_{\mathrm{obs}} | 3\nu), \\ \mathrm{CL_{s+b}} &= P(\Delta\chi^2 \geq \Delta\chi^2_{\mathrm{obs}} | 4\nu), \\ \mathrm{CL_s} &= \frac{\mathrm{CL_{s+b}}}{\mathrm{CL_b}}, \end{aligned} \tag{6}$$

over a grid of $(\sin^2 2\theta_{14}, \Delta m^2_{41})$ points for Daya Bay/Bugey-3 and a grid of $(\sin^2 \theta_{24}, \Delta m^2_{41})$ for MINOS. $\mathrm{CL_b}$ measures consistency with the three-flavor hypothesis, and $\mathrm{CL_{s+b}}$ measures the agreement with the four-flavor hypothesis. The alternate hypothesis is excluded at the $\alpha$ confidence level if $\mathrm{CL_s} \leq 1 - \alpha$. The construction of $\mathrm{CL_s}$ ensures that even if $\mathrm{CL_{s+b}}$ is small, indicating disagreement with the four-flavor hypothesis, this hypothesis can only be excluded when $\mathrm{CL_b}$ is large, indicating consistency with the three-flavor hypothesis. Thus, the $\mathrm{CL_s}$ construction ensures the four-flavor hypothesis can only be excluded if the experiment is sensitive to it.

Calculating $\mathrm{CL_b}$ and $\mathrm{CL_{s+b}}$ can be done in two ways. The first method is the Gaussian $\mathrm{CL_s}$ method [18], which uses two Gaussian $\Delta\chi^2$ distributions. The first distribution assumes the three-flavor hypothesis is true ($\Delta\chi^2_{3\nu}$), and the second assumes the four-flavor hypothesis is true ($\Delta\chi^2_{4\nu}$). The mean of each distribution is obtained from a fit to the Asimov data set, an infinite statistics sample where the relevant parameters are set to best-fit values for each hypothesis [19]. The Gaussian width for the Asimov data set is derived analytically. In the second method, the distributions of $\Delta\chi^2$ are approximated by Monte Carlo (MC) simulations of pseudo-experiments. The Gaussian method is used to obtain the Daya Bay and Bugey-3 combined results, while the second method is used to obtain the MINOS results.

The MINOS experiment [20] operates two functionally equivalent detectors separated by 734 km. The detectors sample the NuMI neutrino beam [21], which yields events with an energy spectrum that peaks at about 3 GeV. Both detectors are magnetized steel/scintillator calorimeters, with the 1 kton Near Detector (ND) situated 1 km downstream of the NuMI production target, and the 5.4 kton Far Detector (FD) located at the Soudan Underground Laboratory [20]. The analysis reported here uses data from an exposure of $10.56 \times 10^{20}$ protons-on-target, for which the neutrino beam composition is 91.8% $\nu_\mu$, 6.9% $\bar{\nu}_\mu$, and 1.3% ($\nu_e + \bar{\nu}_e$).

To look for sterile neutrino mixing, MINOS uses the reconstructed energy spectra in the ND and FD of both charged-current (CC) and neutral-current (NC) neutrino interactions. The sterile mixing signature differs depending on the range of $\Delta m^2_{41}$ values considered. For $\Delta m^2_{41} \in (0.005, 0.05)\ \mathrm{eV}^2$, the muon neutrino CC spectrum in the FD would display deviations from three-flavor oscillations. For rapid oscillations driven by $\Delta m^2_{41} \in (0.05, 0.5)\ \mathrm{eV}^2$,

the combination of finite detector energy resolution and rapid oscillations at the FD location would result in an apparent event rate depletion between the ND and FD. For larger sterile neutrino masses, corresponding to $\Delta m^2_{41} > 0.5\ \mathrm{eV}^2$, oscillations into sterile neutrinos would distort the ND CC energy spectrum. Additional sensitivity is obtained by analyzing the reconstructed energy spectrum for NC candidates. The NC cross sections and interaction topologies are identical for all three active neutrino flavors, rendering the NC spectrum insensitive to standard oscillations, but mixing with a sterile neutrino state would deplete the NC energy spectrum at the FD, as the sterile neutrino would not interact in the detector. For large sterile neutrino masses, such depletion would also be measurable at the ND.

The simulated Far-over-Near ratios of reconstructed energy spectra for $\nu_\mu$ CC and NC selected events, including four-flavor oscillations for both ND and FD, are fit to the equivalent Far-over-Near ratios obtained from data [13]. Current and

previous results of the MINOS sterile neutrino searches, along with further analysis details, are described in [13, 22–24]. MINOS employs the Feldman-Cousins ordering principle [25] in obtaining exclusion limits in the four-flavor parameter space. However, this approach requires a computationally impractical joint fit to be consistent, since it requires minimizing $\chi^2$ over $\Delta m^2_{41}$, a shared parameter between MINOS and Daya Bay/Bugey-3. Thus, the $\mathrm{CL_s}$ method described above is used.

In MINOS, $\sin^2\theta_{34}$ is allowed to vary freely in addition to $\Delta m^2_{32}$ and $\sin^2\theta_{23}$, while $\sin^2\theta_{24}$ and $\Delta m^2_{41}$ are held fixed to define the particular four-flavor hypothesis that is being tested. Since the constraint on $\sin^2\theta_{34}$ is relatively weak, the distribution of $\Delta\chi^2$ deviates from the normal distribution and the Gaussian $\mathrm{CL_s}$ method cannot be used. The $\Delta\chi^2_{3\nu}$ and $\Delta\chi^2_{4\nu}$ distributions are constructed by fitting pseudo-experiments.

In the three-flavor case, pseudo-experiments are simulated using the same parameters listed in [13], *i.e.* $\sin^2\theta_{12} = 0.307$, $\Delta m^2_{21} = 7.54 \times 10^{-5}\,\mathrm{eV}^2$ based on a global fit to neutrino data [26], and $\sin^2\theta_{13} = 0.022$, based on a weighted average of results from reactor experiments [27–29]. For the atmospheric oscillation parameters, equal numbers of pseudo-experiments are simulated in the upper and lower octant ($\sin^2\theta_{23} = 0.61$ and $\sin^2\theta_{23} = 0.41$, respectively), with $|\Delta m^2_{32}| = 2.37 \times 10^{-3}\,\mathrm{eV}^2$, based on the most recent MINOS results [30]. The uncertainties on solar oscillation parameters have negligible effect on the analysis, so fixed values are used. In the four-flavor case, $|\Delta m^2_{32}|$, $\sin^2\theta_{23}$, and $\sin^2\theta_{34}$ are taken from fits to data at each $(\sin^2\theta_{24}, \Delta m^2_{41})$ grid point. In both the three and four-flavor cases, half of the pseudo-experiments are generated in each mass hierarchy. A comparison of MINOS exclusion contours obtained using the Feldman-Cousins procedure [13] with those obtained using the $\mathrm{CL_s}$ method is shown in Fig. 1. Note that if $\Delta m^2_{41} = 2\Delta m^2_{31}$ or $\Delta m^2_{41} \ll \Delta m^2_{31}$ and $\sin^2\theta_{23} = \sin^2\theta_{34} = 1$, $\theta_{24}$ can take on the role normally played by $\theta_{23}$. In these cases, the four-flavor model is degenerate with the three-flavor model, leading to regions of parameter space that cannot be excluded.

The Daya Bay experiment measures electron antineutrinos via inverse beta decay (IBD): $\bar{\nu}_e + p \rightarrow e^+ + n$. The antineutrinos are produced by six reactor cores and detected in eight identical Gd-doped liquid-scintillator detectors (ADs) [31] in three underground experimental halls (EHs). The flux-averaged baselines for EH1, EH2, and EH3 are 520, 570, and 1590 m, respectively. The target mass in each of the two near EHs is 40 tons, and that in the far EH is 80 tons. Details of the IBD event selection, background estimates, and assessment of systematic uncertainties can be found in [27, 32]. By searching for distortions in the $\bar{\nu}_e$ energy spectra, the experiment is sensitive to $\sin^2 2\theta_{14}$ for a mass-splitting $\Delta m^2_{41} \in (0.0003, 0.2)\,\mathrm{eV}^2$. For $\Delta m^2_{41} > 0.2\,\mathrm{eV}^2$, spectral distortions cannot be resolved by the detector. Instead, the measured antineutrino flux can be compared with the predicted flux to constrain the sterile neutrino parameter space. Recently, Daya Bay published its measurement of the overall antineutrino flux [33]. The result is consistent with previous measurements at short baselines, which prefer 5% lower values

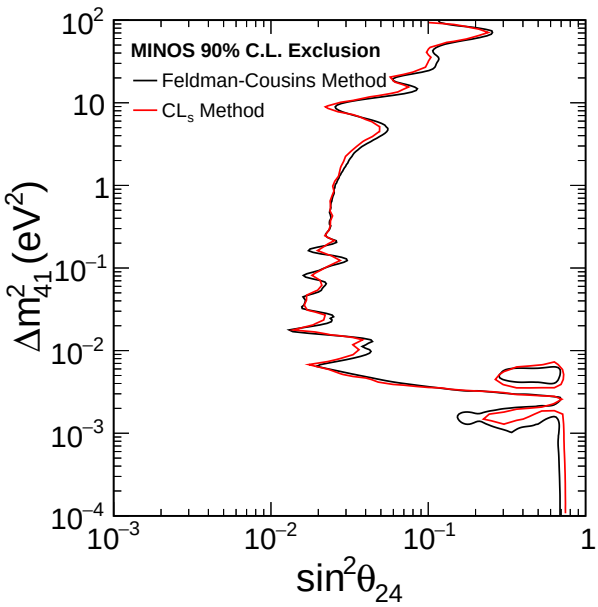


FIG. 1. Comparison of the MINOS 90% C.L. contour using the Feldman-Cousins method [13] and the $\mathrm{CL_s}$ method. The region to the right of the curve is excluded at the 90% C.L.

than the latest calculations [34, 35], a deficit commonly referred to as the reactor antineutrino anomaly [36]. However, the reactor spectrum measurement from Daya Bay [33] (and from RENO [28] and Double Chooz [29]) shows clear discrepancies with the latest calculations, which indicates an underestimation of their uncertainties. The uncertainties on the antineutrino flux models for this analysis are increased to 5% from the original 2% as suggested by [37, 38].

The Daya Bay Collaboration has recently updated the sterile neutrino search result in [12] with limits on $\sin^2 2\theta_{14}$ improved by about a factor of two with respect to previous results [39]. This data set is used in producing the combined results presented here.

Two independent sterile neutrino search analyses are conducted by Daya Bay. The first analysis uses the predicted $\bar{\nu}_e$ spectrum to generate the predicted prompt spectrum for each AD simultaneously, taking into account detector effects such as energy resolution, nonlinearity, detector efficiency, and oscillation parameters described in [27]. A log-likelihood function is constructed with nuisance parameters to include the detector-related uncertainties and a covariance matrix to incorporate the uncertainties on reactor neutrino flux prediction. The Gaussian $\mathrm{CL}_s$ method is used to calculate the excluded region. The second analysis uses the observed spectra at the near sites to predict the far site spectra to further reduce the dependency on reactor antineutrino flux models. Both analyses yield consistent results [12].

The Bugey-3 experiment was performed in the early 1990s and its main goal was to search for neutrino oscillations using reactor antineutrinos. In this experiment, two $^6$Li-doped

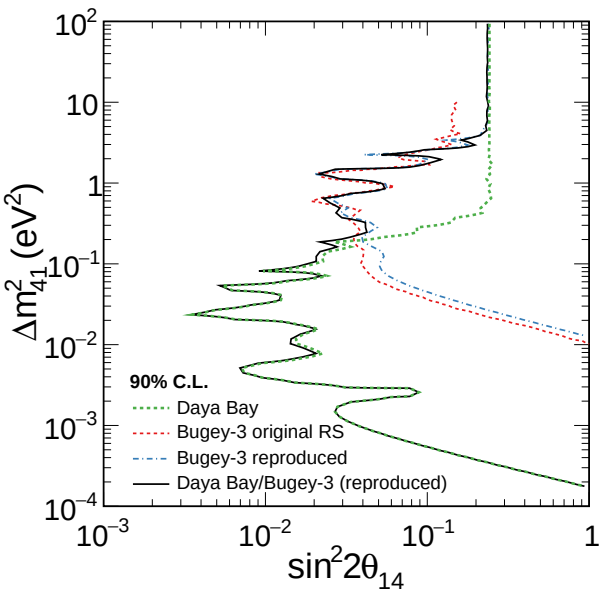


FIG. 2. Excluded regions for the original Bugey-3 raster scan (RS) result [14], for the reproduced Bugey-3 with adjusted fluxes, for the Daya Bay result [12], and for the combined Daya Bay and reproduced Bugey-3 results. The region to the right of the curve is excluded at the 90% C.L.

liquid scintillator detectors measured $\bar{\nu}_e$ generated from two reactors at three different baselines (15, 40 and 95 m) [14]. Bugey-3 detected IBD interactions with the recoil neutron capturing on $^6$Li (n + $^6$Li $\rightarrow$ $^4$He + $^3$H + 4.8 MeV). Probing shorter baselines than Daya Bay, Bugey-3 is sensitive to regions of parameter space with larger $\Delta m^2_{41}$ values.

The original Bugey-3 results obtained using the raster scan technique are first reproduced employing a $\chi^2$ definition used in the original Bugey-3 analysis [14]:

$$\chi^2 = \sum_i^3 \sum_j^{N_i} \frac{\left[(Aa_i + b(E_j - 1.0))\, R^{\rm pre}_{i,j} - R^{\rm obs}_{i,j}\right]^2}{\sigma^2_{i,j}} + \sum_i^3 \frac{(a_i - 1)^2}{\sigma^2_{a_i}} + \frac{(A-1)^2}{\sigma^2_A} + \frac{b^2}{\sigma^2_b}, \quad (7)$$

where $A$ is the overall normalization, $a_i$ is the relative detection efficiency, $b$ is an empirical factor to include the uncertainties of the energy scale, $i$ represents the data from three baselines, and $j$ sums over the $N_i$ bins at each baseline. The values of $\sigma_{a_i}$ and $\sigma_b$ are set at 0.014 and 0.020/MeV, respectively, according to the reported values in [14]. The $\sigma_{i,j}$ are the statistical uncertainties. The uncertainty on the overall normalization $\sigma_A$ is set to 5% to be consistent with the constraint employed in the Daya Bay analysis [12]. The ratio of the observed spectrum to the predicted unoscillated spectrum is denoted by $R^{\rm obs}_{i,j}$, while $R^{\rm pre}_{i,j}$ is the predicted ratio of the spectrum including oscillations to the one without oscillations. To predict the energy spectra, the average fission fractions are used [40], and the energy resolution is set to 5% at 4.2 MeV [14] with a functional form similar to Daya Bay's. The predicted energy spectra are validated against the published Bugey-3 spectra [14].

In Bugey-3, the change in the oscillation probability over the size of the detectors and the reactors is studied with MC assuming that antineutrinos are uniformly generated in the reactor cores and uniformly measured in the detectors, and approximated by treating the baselines as normal distributions. To achieve the combination with Daya Bay, two changes are made in the reproduced Bugey-3 analysis: the change in cross section of the IBD process due to the updated neutron decay time [6] is applied; and the antineutrino flux is adjusted from the ILL+Vogel model [41, 42] to that of Huber [34] and Mueller [35], for consistency with the prediction used by Daya Bay. These adjustments change the reproduced contour with respect to the original Bugey-3 one, in particular by reducing sensitivity to regions with $\Delta m^2_{41} > 3\,\mathrm{eV}^2$, with less noticeable effects for smaller $\Delta m^2_{41}$ values. The reproduced Bugey-3 limit on the sterile neutrino mixing, and the limit obtained by combining Bugey-3 with Daya Bay results through a $\chi^2$ fit, with common overall normalization and oscillation parameters, are shown in Fig. 2.

Individually, MINOS and Bugey-3 are both sensitive to regions of parameter space allowed by the LSND measurement through constraints on $\theta_{14}$ and $\theta_{24}$, shown in Fig. 2 and Fig. 1, respectively. We illustrate this sensitivity in Fig. 3, which displays a comparison of the energy spectra for Bugey-3 and MINOS data to four-flavor predictions produced at the LSND best-fit point of ($\Delta m^2_{41} = 1.2$ eV$^2$, $\sin^2 2\theta_{\mu e} = 0.003$) [8].

In our combined analysis, we obtain $\Delta\chi^2_{\rm obs}$, as well as $\Delta\chi^2_{3\nu}$ and $\Delta\chi^2_{4\nu}$ distributions for each $(\sin^2 2\theta_{14}, \Delta m^2_{41})$ grid point of the Daya Bay and Bugey-3 combination, and for each $(\sin^2\theta_{24}, \Delta m^2_{41})$ grid point from MINOS. We then combine pairs of grid points from the MINOS and the Daya Bay/Bugey-3 results at fixed values of $\Delta m^2_{41}$ to obtain constraints on electron neutrino or antineutrino appearance due to oscillations into sterile neutrinos. Since the systematic uncertainties of accelerator and reactor experiments are largely uncorrelated, for each $(\sin^2 2\theta_{14}, \sin^2\theta_{24}, \Delta m^2_{41})$ grid point, a combined $\Delta\chi^2_{\rm obs}$ is constructed from the sum of the corresponding MINOS and Daya Bay/Bugey-3 $\Delta\chi^2_{\rm obs}$ values. Similarly, the combined $\Delta\chi^2_{3\nu}$ and $\Delta\chi^2_{4\nu}$ distributions are constructed by adding random samples drawn from the corresponding MINOS and Daya Bay/Bugey-3 distributions. Finally, the $\mathrm{CL_s}$ value at every $(\sin^2 2\theta_{14}, \sin^2\theta_{24})$ point is calculated using Eq. (6), while the $\Delta m^2_{41}$ value is fixed. While $\mathrm{CL_s}$ is single-valued at every $(\sin^2 2\theta_{14}, \sin^2\theta_{24})$ point for a given value of $\Delta m^2_{41}$, it is multi-valued as a function of $\sin^2 2\theta_{\mu e}$ (*cf.* Eq. (5)). To obtain a single-valued function, we make the conservative choice of selecting the largest $\mathrm{CL_s}$ value for any given $\sin^2 2\theta_{\mu e}$. The 90% C.L. exclusion contour resulting from this procedure is shown in Fig. 4. Under the assumption of CPT conservation, the combined constraints are equally valid in constraining electron neutrino or antineutrino appearance. The

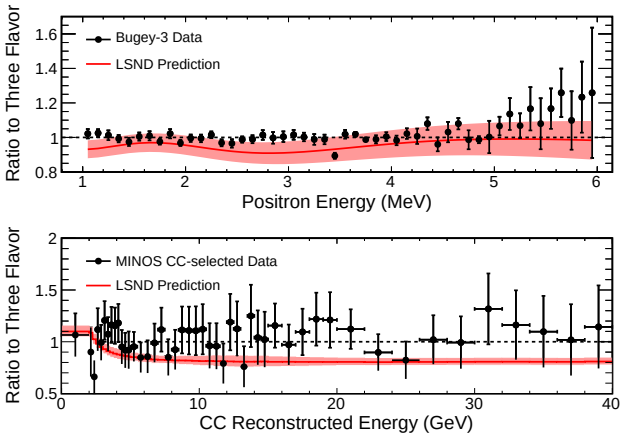


FIG. 3. The top panel shows the ratio of the Bugey-3 15 m IBD data to a three-neutrino prediction, while the bottom panel shows the ratio of the MINOS Far-over-Near data for CC events to a three-neutrino prediction. The red lines represent the four-flavor predictions at the LSND best-fit point for $\Delta m^2_{41} = 1.2$ eV$^2$. The shaded band displays the sizes of the systematic uncertainties. A value of $\sin^2 2\theta_{14} = 0.11$ is used for the Bugey-3 prediction so that when multiplied by the MINOS 90% C.L. limit on $\sin^2\theta_{24}$, as in Eq. 5, it matches the LSND best-fit of $\sin^2 2\theta\mu e = 0.003$. A $\Delta\chi^2$ value of 48.2 is found between the data and the LSND prediction. Similarly, a value of $\sin^2\theta_{24} = 0.12$ is combined with the Bugey-3 90% C.L. limit on $\theta_{14}$ to produce the MINOS four-flavor prediction, resulting in $\Delta\chi^2 = 38.0$ between data and prediction.

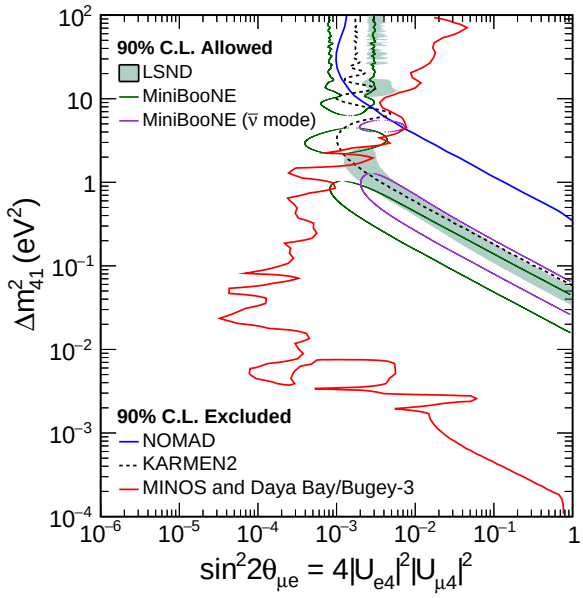


FIG. 4. MINOS and Daya Bay/Bugey-3 combined 90% C.L. limit on $\sin^2 2\theta_{\mu e}$ compared to the LSND and MiniBooNE 90% C.L. allowed regions. Regions of parameter space to the right of the red contour are excluded. The regions excluded at 90% C.L. by KARMEN2 [43] and NOMAD [44] are also shown.

combined results of Daya Bay/Bugey-3 and MINOS constrain $\sin^2 2\theta_{\mu e} < [3.0 \times 10^{-4}$ (90% C.L.), $4.5 \times 10^{-4}$ (95% C.L.)] for $\Delta m^2_{41} = 1.2$ eV$^2$. While the results do not exclude the MiniBooNE neutrino-mode best-fit point ($\Delta m^2_{41} = 3.14$ eV$^2$, $\sin^2 2\theta_{\mu e} = 0.002$) [9] at the 90% C.L., they do exclude the LSND best-fit point ($\Delta m^2_{41} = 1.2$ eV$^2$, $\sin^2 2\theta_{\mu e} = 0.003$) [8] and the MiniBooNE antineutrino-mode best-fit point ($\Delta m^2_{41} = 0.043$ eV$^2$, $\sin^2 2\theta_{\mu e} = 0.88$) [9] at greater than $3\sigma$.

In conclusion, we have combined constraints on $\sin^2 2\theta_{14}$ derived from a search for electron antineutrino disappearance at the Daya Bay and Bugey-3 reactor experiments with constraints on $\sin^2\theta_{24}$ derived from a search for muon (anti)neutrino disappearance in the NuMI beam at the MINOS experiment. Assuming a four-flavor model of active-sterile oscillations, we constrain $\sin^2 2\theta_{\mu e}$, the parameter controlling electron (anti)neutrino appearance at short-baseline experiments, over six orders of magnitude in $\Delta m^2_{41}$. We set the strongest constraint to date and exclude the sterile neutrino mixing phase space allowed by the LSND and MiniBooNE experiments for $\Delta m^2_{41} < 0.8$ eV$^2$ at a 95% C.L. These results increase the strong tension between null results from disappearance searches and appearance-based indications for the existence of light sterile neutrinos.

The MINOS experiment is supported by the U.S. Department of Energy; the United Kingdom Science and Technology Facilities Council; the U.S. National Science Foundation; the State and University of Minnesota; and Brazil's FAPESP (Fundação de Amparo à Pesquisa do Estado de São Paulo), CNPq (Conselho Nacional de Desenvolvimento Científico e Tecnológico), and CAPES (Coordenação de Aperfeiçoamento de Pessoal de Nível Superior). We are grateful to the Minnesota Department of Natural Resources and the personnel of the Soudan Laboratory and Fermilab. We thank the Texas Advanced Computing Center at The University of Texas at Austin for the provision of computing resources.

The Daya Bay experiment is supported in part by the Ministry of Science and Technology of China; the U.S. Department of Energy; the Chinese Academy of Sciences; the CAS Center for Excellence in Particle Physics; the National Natural Science Foundation of China; the Guangdong provincial government; the Shenzhen municipal government; the China General Nuclear Power Group; the Research Grants Council of the Hong Kong Special Administrative Region of China; the Ministry of Education in Taiwan; the U.S. National Science Foundation; the Ministry of Education, Youth and Sports of the Czech Republic; the Joint Institute of Nuclear Research in Dubna, Russia; the NSFC-RFBR joint research program; and the National Commission for Scientific and Technological Research of Chile. We acknowledge Yellow River Engineering Consulting Co., Ltd. and China Railway 15th Bureau Group Co., Ltd. for building the underground laboratory. We are grateful for the ongoing cooperation from the China Guangdong Nuclear Power Group and China Light & Power Company.

* Deceased.
† Now at Department of Chemistry and Chemical Technology, Bronx Community College, Bronx, New York 10453, USA

[1] Y. Fukuda *et al.* (Super-Kamiokande), Phys. Rev. Lett. **81**, 1562 (1998).
[2] Q. R. Ahmad *et al.* (SNO), Phys. Rev. Lett. **87**, 071301 (2001).
[3] B. Pontecorvo, Sov. Phys. JETP **6**, 429 (1957).
[4] B. Pontecorvo, Sov. Phys. JETP **26**, 984 (1968).
[5] Z. Maki, M. Nakagawa, and S. Sakata, Prog. Theor. Phys. **28**, 870 (1962).
[6] K. Olive *et al.* (Particle Data Group), Chinese Phys. C **38**, 090001 (2014).
[7] S. Schael *et al.* (ALEPH , DELPHI , L3 , OPAL , SLD , LEP Electroweak Working Group, SLD Electroweak Group, SLD Heavy Flavour Group), Phys. Rept. **427**, 257 (2006).
[8] A. Aguilar *et al.* (LSND), Phys. Rev. D **64**, 112007 (2001).
[9] A. Aguilar-Arevalo *et al.* (MiniBooNE), Phys. Rev. Lett. **110**, 161801 (2013).
[10] K. Abazajian *et al.*, arXiv:1204.5379 [hep-ph].
[11] J. Kopp, P. A. N. Machado, M. Maltoni, and T. Schwetz, JHEP **05**, 050 (2013).
[12] F. P. An *et al.* (Daya Bay), (2016), submitted to Phys. Rev. Lett., arXiv:1607.01174 [hep-ex].
[13] P. Adamson *et al.* (MINOS), (2016), submitted to Phys. Rev. Lett., arXiv:1607.01176 [hep-ex].
[14] B. Achkar *et al.*, Nucl. Phys. B **434**, 503 (1995).
[15] A. L. Read, J. Phys. G **28**, 2693 (2002).
[16] T. Junk, Nucl. Instrum. Meth. A **434**, 435 (1999).
[17] H. Harari and M. Leurer, Phys. Lett. **B181**, 123 (1986).
[18] X. Qian, A. Tan, J. J. Ling, Y. Nakajima, and C. Zhang, Nucl. Instrum. Meth. A **827**, 63 (2016).
[19] G. Cowan, K. Cranmer, E. Gross, and O. Vitells, Eur. Phys. J. C **71**, 1554 (2011), [Erratum: Eur. Phys. J. C **73**, 2501 (2013)].
[20] D. G. Michael *et al.* (MINOS), Nucl. Instrum. Meth. A **596**, 190 (2008).
[21] P. Adamson *et al.* (MINOS), Nucl. Instrum. Meth. A **806**, 279 (2016).
[22] P. Adamson *et al.* (MINOS), Phys. Rev. Lett. **107**, 011802 (2011).
[23] P. Adamson *et al.* (MINOS), Phys. Rev. D **81**, 052004 (2010).
[24] P. Adamson *et al.* (MINOS), Phys. Rev. Lett. **101**, 221804 (2008).
[25] G. J. Feldman and R. D. Cousins, Phys. Rev. D **57**, 3873 (1998).
[26] G. L. Fogli, E. Lisi, A. Marrone, D. Montanino, A. Palazzo, and A. M. Rotunno, Phys. Rev. D **86**, 013012 (2012).
[27] F. P. An *et al.*, Phys. Rev. Lett. **115**, 111802 (2015).
[28] J. H. Choi *et al.* (RENO), Phys. Rev. Lett. **116**, 211801 (2016).
[29] Y. Abe *et al.* (Double Chooz), JHEP **10**, 086 (2014), [Erratum: JHEP **02**, 074 (2015)].
[30] P. Adamson *et al.* (MINOS), Phys. Rev. Lett. **112**, 191801 (2014).
[31] F. P. An *et al.* (Daya Bay), Nucl. Instrum. Meth. A **811**, 133 (2016).
[32] F. An *et al.* (Daya Bay), Phys. Rev. Lett. **112**, 061801 (2014).
[33] F. P. An *et al.* (Daya Bay), Phys. Rev. Lett. **116**, 061801 (2016).
[34] P. Huber, Phys. Rev. C **84**, 024617 (2011), [Erratum: Phys. Rev. C **85**, 029901 (2012)].
[35] T. A. Mueller *et al.*, Phys. Rev. C **83**, 054615 (2011).
[36] G. Mention *et al.*, Phys. Rev. D **83**, 073006 (2011).
[37] A. Hayes, J. Friar, G. Garvey, G. Jungman, and G. Jonkmans, Phys. Rev. Lett. **112**, 202501 (2014).
[38] P. Vogel (2016) arXiv:1603.08990 [hep-ph].
[39] F. An *et al.*, Phys. Rev. Lett. **113**, 141802 (2014).
[40] Y. Declais *et al.*, Phys. Lett. B **338**, 383 (1994).
[41] K. Schreckenbach *et al.*, Phys. Lett. B **160**, 325 (1985).
[42] P. Vogel, Phys. Rev. D **29**, 1918 (1984).
[43] B. Armbruster *et al.* (KARMEN), Phys. Rev. D **65**, 112001 (2002).
[44] P. Astier *et al.* (NOMAD), Phys. Lett. B **570**, 19 (2003).

Note Added: Following completion of this manuscript, a paper submitted by the IceCube Collaboration that sets limits using sterile-driven disappearance of muon neutrinos has been accepted for publication (see arXiv:1605.01990 [hep-ex]). The results place strong constraints on $\sin^2 2\theta_{24}$ for $\Delta m^2_{41} \in (0.1, 10)\ \mathrm{eV}^2$. Further, a paper that re-analyses the same IceCube data in a model including non-standard neutrino interactions has also been accepted for publication (see arXiv:1602.08766 [hep-ex]).